Earth and Planetary Science Letters, 60 (1982)178–194
Elsevier Scientific Publishing Company, Amsterdam – Printed in The Netherlands

[6]

A parameterized model for the evolution of isotopic heterogeneities in a convecting system

Frank M. Richter [1], Stephen F. Daly [2] and Henri-Claude Nataf [3]

[1] *Department of Geophysical Sciences, University of Chicago, Chicago, IL 60637 (U.S.A.)*
[2] *Jet Propulsion Laboratory, California Institute of Technology, Pasadena, CA 91109 (U.S.A.)*
[3] *Seismological Laboratory, California Institute of Technology, Pasadena, CA 91125 (U.S.A.)*

Received December 22, 1981
Revised version received May 24, 1982

Laboratory experiments are used to illustrate how steady convective flows, while efficient at stirring an initial heterogeneity within a single cell, do not produce dispersal of heterogeneous material over scales large compared to the depth. Long-range dispersal requires that the flow be time dependent on a time scale comparable to the overturn time. Convection in an internally heated layer has this property and numerical solutions are used to study the way in which it disperses a set of neutrally buoyant particles that were initially confined to a small space. The horizontal dispersal of these particles is reasonably well represented by an effective diffusivity of 0.3 cm^2/s for a Rayleigh number of 10^6. The concept of an effective diffusivity is then applied to the isotopic evolution of the Sm-Nd and Rb-Sr systems with spatial variations generated by horizontal variations in degree of melting 1.8×10^9 years ago. The present-day average ϵ value one would measure in such a system depends on the average degree of melting, the amplitude and length scale of variations in partial melt, and the effective diffusivity assumed. Especially in the case of Nd the differences in average ϵ value between a uniform and a spatially variable (but with the same average) melting case can be significant. The range of ϵ values about the average is controlled by the competing effects of generation by the differences in enrichment factor and decay due to the effective diffusivity.

1. Introduction

Considerable progress has been made in recent years in characterizing the source material of mid-ocean ridge basalts (MORB). Because of their pervasiveness, these basalts are generally believed to provide the best measure of the chemical properties of the upper mantle, especially in the case of its isotopic composition. The isotopic composition of Nd is central to most recent chemical evolution arguments because of the greater confidence with which the bulk earth parent to daughter ratio can be assumed. Also the observed correlation of $^{143}Nd/^{144}Nd$ with $^{87}Sr/^{86}Sr$ [1–4] gives hope that the isotopic systems are not complicated beyond successful modelling. Fig. 1 shows this remarkable correlation (the mantle array) in terms of ϵ_{Nd} and ϵ_{Sr}, which measure departures of the isotopic ratios from a reference state taken as chondritic for Sm-Nd.

Some aspects of the Nd and Sr isotopic data have received much attention. The average isotopic composition of MORB ($\epsilon_{Nd} \sim 10$, $\epsilon_{Sr} \sim -27$) is most often explained as resulting from the extraction by partial melting of the continental crust from some or all of the mantle, leaving a depleted residual mantle that will yield the MORB values upon remelting. Jacobsen and Wasserburg [5] for example modelled such a situation and found that the volume of mantle involved is about 1/3 the total and that the mean age of extraction (mean age of the continents) is 1.8×10^9 years. The emphasis in such models is to explain the average ϵ values in terms of the average properties of the

0012-821X/82/0000–0000/$02.75

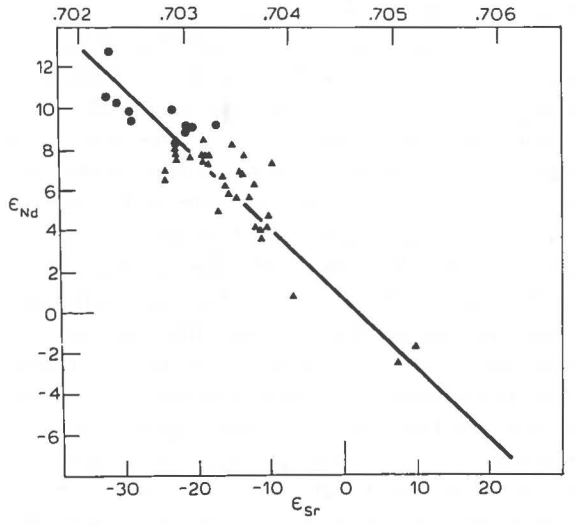

Fig. 1. Correlation of ϵ_{Nd} with ϵ_{Sr} for oceanic basalts taken from DePaolo and Wasserburg [22]. The circles are MORB and the triangles are ocean island basalts.

various geochemical reservoirs assumed to be involved. We show below that the average of a set of ϵ values has different interpretations depending on the heterogeneity of the system and the efficiency of convective stirring.

The mantle array can be explained in terms of mixing depleted mantle (upper mantle) with mantle material that was not involved in the generation of the continental crust [6]. Alternatively the mantle array could have been generated by the evolution of the continental crust through time if a nearly uniform ratio of the enrichment factors of Sm-Nd to Rb-Sr is left behind. DePaolo [7] and Allègre et al. [8] point out some of the special requirements such an explanation places on the melting process, further special circumstances are required in order that MORB always represent an extreme composition along the mantle array. In the case of the mantle array, the emphasis is on processes that yield a linear or almost linear correlation and little attention is given to the scatter of the data, which is small but somewhat larger than analytical errors. It could be argued that the scatter is small due to efficient stirring by mantle convection but this idea needs quantitative study lest it lead also to the "homogenization" of the points along the mantle array.

Little besides heuristic arguments exist as to the effect of thermal convection on the evolution of isotopic heterogeneities in a system such as the mantle. Convection can be ignored only when modelling the averaged properties of mantle reservoirs and even then some statement regarding the convective processes is required to predict the average ϵ values that would be measured. The scaling arguments in Richter and Ribe [9] suggest that convection becomes a crucial process once the velocities exceed a few millimeters per year, and velocities considerably in excess of this are generally believed to exist in the mantle. The stirring of passive chemical heterogeneities (those that do not affect density) was discussed by Richter and Ribe [9] in the special case of two-dimensional, steady convection cells. Under these restricted conditions any original heterogeneity of finite size will with time take the shape of an increasingly tightly wound spiral, but no material is exchanged between cells. We illustrate this behavior by means of laboratory experiments described in the next section. In a general way one can characterize such stirring as efficient on the scale of individual cells but incapable of producing dispersal over larger horizontal scales. Dispersal of a passive tracer over horizontal scales large compared to the cells themselves requires time dependence, which we demonstrate first with a system in which closed cells migrate with a prescribed phase speed and then with a numerical example of internally heated convection. The dispersal seen in the latter case can be represented in terms of an effective diffusivity (~ 0.3 cm^2/s), a concept we then use in a simple model for the evolution of isotopic variations in a parameterized convecting system.

2. Stirring by steady convective flows

Laboratory experiments were carried out in which neutrally buoyant dye was injected into a layer of convecting silicone oil contained between horizontal, isothermal glass boundaries that allow the dispersal of the dye to be observed. The simplest cases are those at low Rayleigh number ($< 2 \times 10^4$) in which the flow is two-dimensional rolls. Fig. 2 shows the evolution of dye in such a situa-

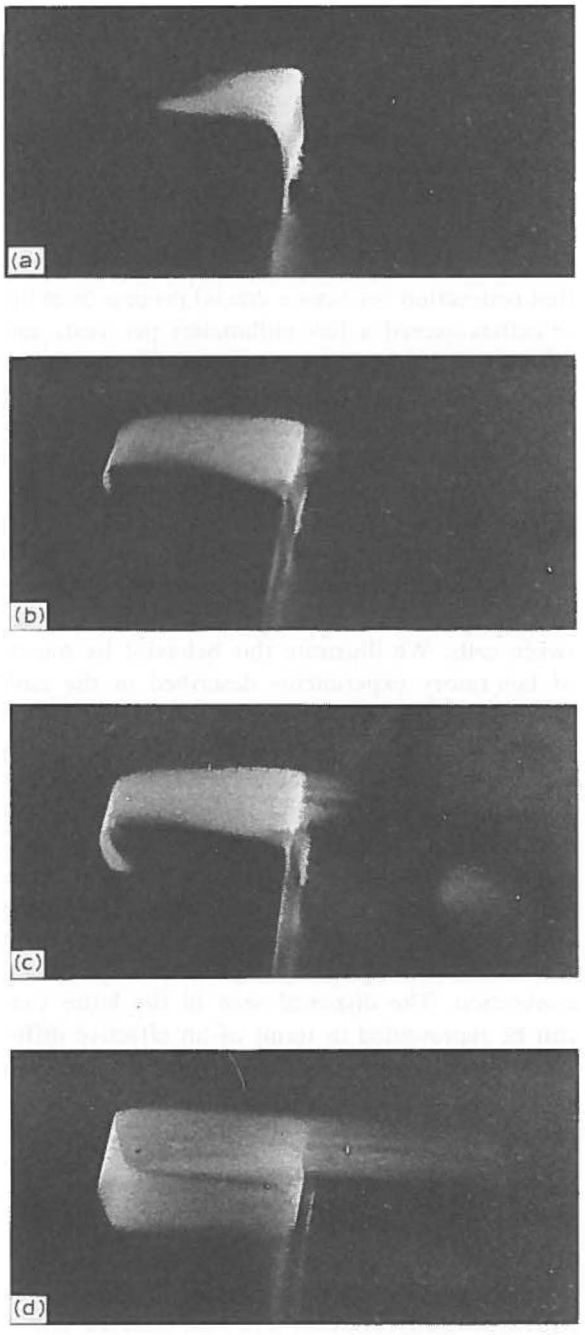

Fig. 2. Evolution of dye, appearing white in this photograph, in the case of convection rolls. The dye was introduced by a thin tube into the upwelling sheat. The photographs are looking downwards at 45° and along the axis of the (unseen initially) roll to the right of the one containing most of the dye.

tion. The camera is looking downwards at 45° along the axis of the unseen roll immediately to the right of the cell containing most of the dye. The dye was injected at the base of the upwelling and by the time of picture (a) it has risen to the top boundary and begun to move horizontally. By (d) the first overturn is complete and a second sheet of dye is beginning to develop in a way similar to that described in Richter and Ribe [9]. A small amount of dye is by this time spreading along the cell on the right but the velocities are much slower because the dye is along streamlines close to the stationary upper boundary. The point of these photographs is that they illustrate how an originally more or less spherical "heterogeneity" becomes stretched out into spiral sheets. Some experiments included an imposed shear along the axis of the cells representing a possible mantle situation with rolls aligned in the direction of the return flow under a moving lithospheric plate as suggested by Richter [10] and Richter and Parsons [11]. In such cases, the dye streaks become quite complicated but in general can be characterized as cork screw patterns with axis in the direction of shear. With time, the dye streaks are contained in a band one cell width wide and down stream of the original point of injection.

At the higher Rayleigh numbers characteristic of the mantle ($Ra > 10^6$) the platform of convection is the spoke pattern shown by means of a shadowgraph in Fig. 3d. The cells are irregular polygons with rising (sinking) sheets radiating out of a central upwelling (downwelling) and the characteristic scale is of the order of the depth of the layer. Photographs (a), (b) and (c) show both the shadowgraph and the actual dye which is in a layer about 5 cm above the plane of the shadowgraph. The relationship between the dyed layer and the shadowgraph is best seen in (a) where dye is being injected through a thin tube into the central upwelling of a cell. In (b) the dye has risen to the top of the cell and perfectly outlines its horizontal extent. By (c) dye is sinking along the sides. Eventually the dye pattern is a large number of filaments within a single cell and radiating out of the central upwelling. Photograph (d) is a shadowgraph alone taken at a later time. The cell of the preceding photographs can be seen and also

another cell in which the dye remains confined to a wedge-shaped sector of a polygonal cell. These experiments show how a "heterogeneity" will become drawn out but for the most part remains within a single cell or portion of a cell, even at high Rayleigh number.

In general, steady convective flows can be effective at dispersing an original "heterogeneity" throughout the depth of the layer and on a horizontal scale comparable to the depth. If shear is added, dispersal in the direction of the shear takes place but the cross-shear dispersal is still limited. The dispersal of a "heterogeneity" over scales large compared to the depth requires time dependence, which is the subject taken up in the next two sections.

3. The effect of time dependence

The effect of time dependence on the dispersal of passive tracers can be illustrated by considering the trajectories of marked particles in a simple two-dimensional flow with closed streamlines that migrates with time. The velocity field $\underset{\sim}{u}(x, z, t)$ assumed for this purpose is:

$$\underset{\sim}{u} = \frac{\partial \psi}{\partial z}\hat{i} - \frac{\partial \psi}{\partial x}\hat{k} \tag{1}$$

where $\hat{i}$ and $\hat{k}$ are unit vectors in the x and z direction and the stream function $\psi(x, z, t)$ is given by:

$$\psi = A \sin \pi z \sin(mx - \sigma t) \tag{2}$$

The streamlines are closed cells at any instant in time regardless of σ which controls the phase. The trajectory $(X(t), Z(t))$ of a particle originally at (x_0, z_0) is found by integrating:

$$\frac{dX}{dt} = \left.\frac{\partial \psi}{\partial z}\right|_{X,Z} \tag{3}$$

$$\frac{dZ}{dt} = -\left.\frac{\partial \psi}{\partial x}\right|_{X,Z} \tag{4}$$

Analytic solutions of (3) and (4) are not generally obtainable because the right-hand side needs to be evaluated at the unknown position $X(t)$, $Z(t)$; but limiting cases and numerical solutions of sufficient accuracy are easily obtained.

Case $\sigma/m \to 0$. This limit represents the steady case studied by Richter and Ribe [9] and the trajectories are along streamlines. Since the streamlines are closed, material within a cell never leaves it. An original heterogeneity will with time become drawn out into a spiral since (2) does not represent rigid body rotation. Examples of the relative motion of particles in this limit but with more realistic streamlines obtained from numerical solutions of the convective equations can be found in work by McKenzie [12].

Case $\sigma/m \to \infty$. This limit of very rapid translation of the streamline pattern has an approximate solution:

$$X(t) = x_0 + \frac{A\pi}{\sigma}\cos \pi z_0 \{\cos(mx_0 - \sigma t) - \cos(mx_0)\} \tag{5}$$

$$Z(t) = z_0 + \frac{Am}{\sigma}\sin \pi z_0 \{\sin(mx_0 - \sigma t) - \sin(mx_0)\} \tag{6}$$

The trajectories are ellipses with axis of order $1/\sigma$, therefore particles do not disperse since they remain very close to their original position. O'Connell and Hager [13] have argued that the rapid migration of ridges can result in a relatively isolated lower mantle, a suggestion related to the limit discussed here where sufficiently fast time dependence inhibits dispersal. Their argument is kinematically sound given sufficient time dependence but dynamically unlikely because the isolated material will warm up, become less dense and finally rise ending its isolation. The point is that kinematic arguments can serve only as guides and realistic models of convective stirring must include the buoyancy forces maintaining the flow.

Case $\sigma/m = A$. This regime of phase speed comparable to the convective velocity does lead to dispersal over distances large compared to the size of individual cells. Fig. 4 is an example of the dispersal of two particles, initially in the same cell, when $\sigma/m = A$. The streamlines at three different times are shown together with the trajectory of each particle. The position of the two particles at

each time is marked by a + on the trajectory. A stationary observer sees the two particles moving in opposite directions from which he concludes that a "heterogeneity" of sufficient size would be stretched out over large distances.

In general, long-range dispersal will occur when

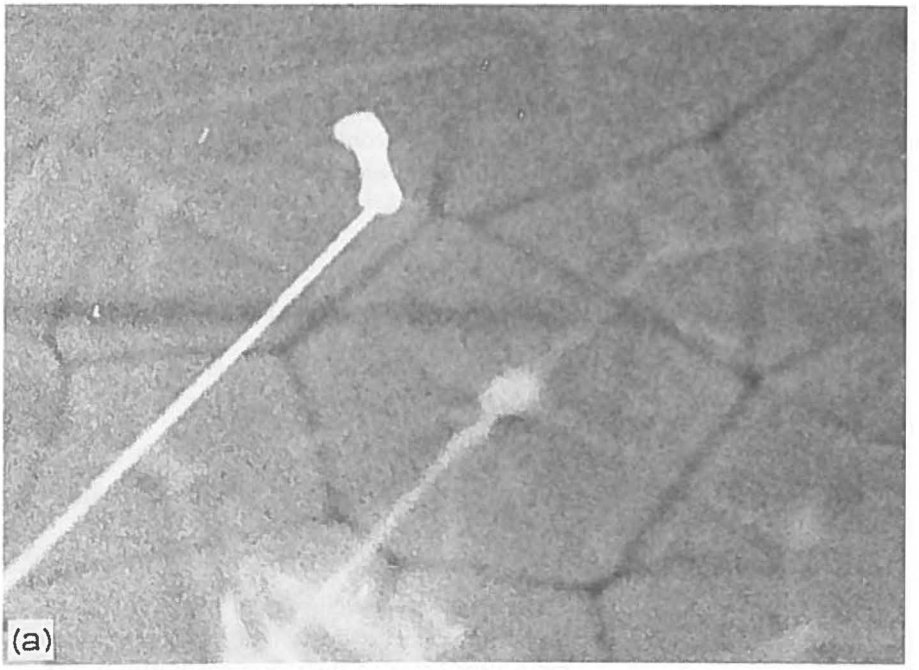

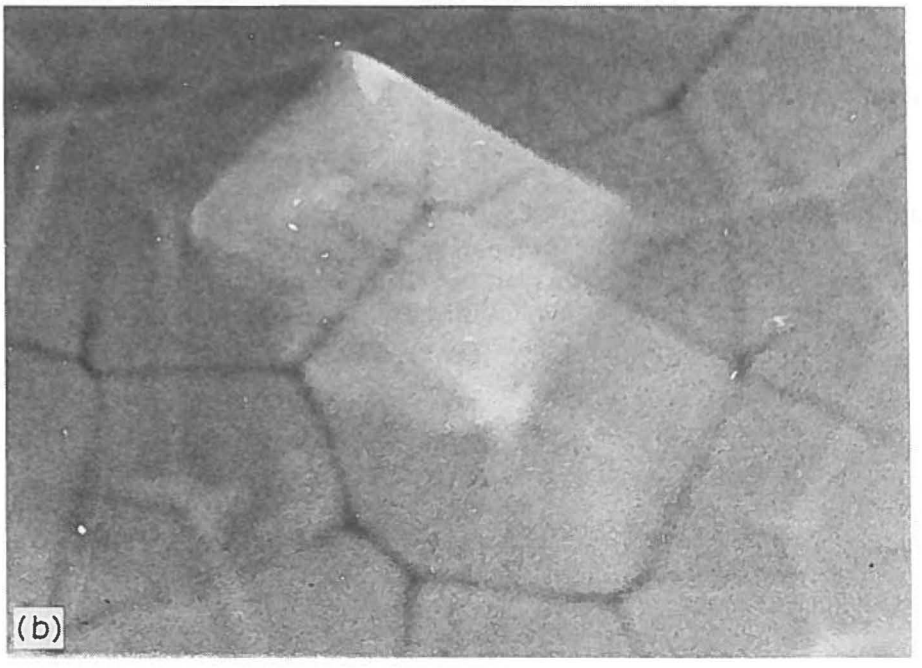

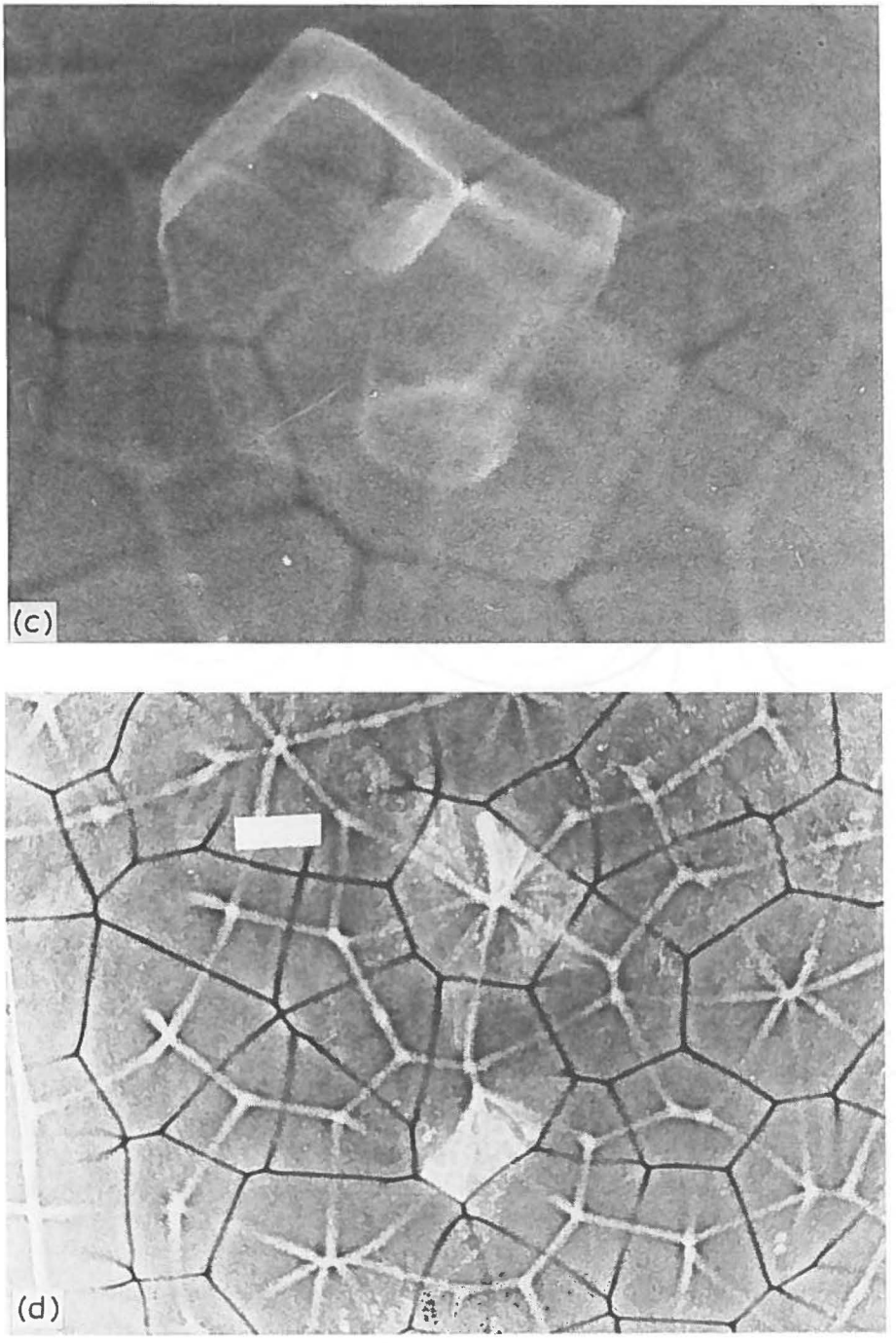

Fig. 3. Dye pattern and shadowgraph of spoke convection. The dye is injected into the central upwelling of a cell through a thin tube that can be seen in (a). The shadowgraph, in which cold sinking regions appear as dark lines and rising regions are the fainter light lines, is in a plane about 5 cm below the actual fluid layer. Photograph (d) is a shadowgraph alone showing more of the cells and how dye (light colored) is pretty much confined to single cells. The almost pentagonal cell to the right of the white rectangle (whose long dimension is equal to the depth of the layer) is the one shown in detail in the other photographs. The more or less triangular region of dye in the cell below it, is from an earlier experiment and the dye is seen to be very confined even after about 30 turnover times.

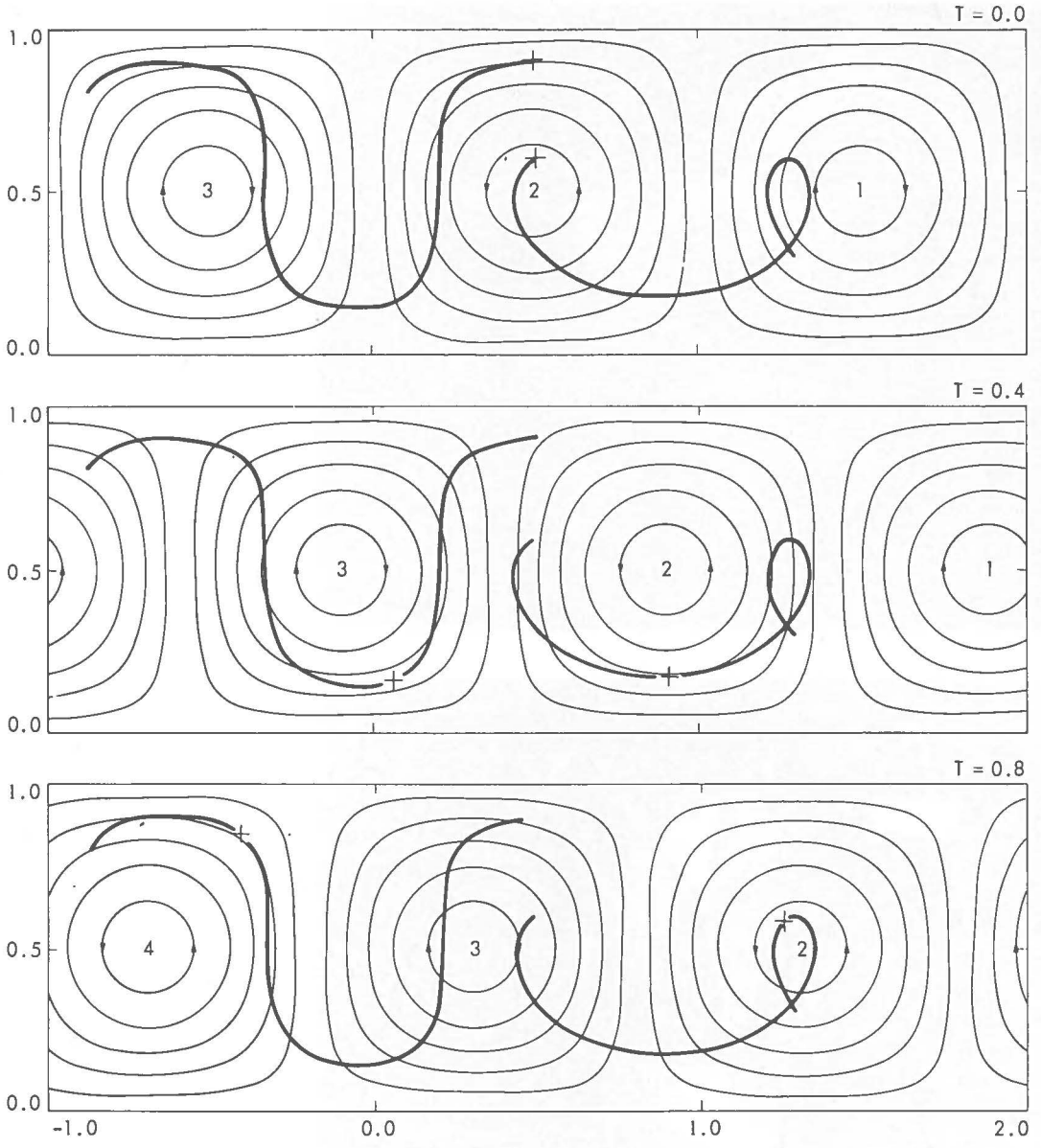

Fig. 4. Streamlines and the trajectories of two particles in the case $\sigma/m = A$. The dark line is the trajectory and the cross is the position along the trajectory of the two particles at the three times given. Time is in units A^{-1}.

the phase speed of a convective pattern is comparable to the convective velocities themselves. Put differently, the condition is that the characteristic time scale associated with the time dependence should be comparable to the overturn time, a requirement met by the numerical solutions for convection in internally heated fluids [14,15].

4. Stirring by internally heated convection

Numerical solutions for two-dimensional internally heated convection become time dependent at Rayleigh numbers comparable to those expected for the upper mantle and we use these to illustrate the dispersal of a set of marked particles over

distances large compared to the depth of the system. At least for this particular type of convection the observed dispersal can be parameterized in terms of a horizontal effective diffusivity, which in turn leads to a description of how isotopic heterogeneities will evolve in a gross sense. A more realistic upper mantle convection model would be one in which the separate lower mantle is internally heated while the upper mantle is depleted of heat producing elements and thus driven almost entirely by the flux of heat from below [16]. In such a layered system the flow is also time dependent [17] and a similar result in terms of effective dispersal would be found.

The streamlines and temperature field at various times for a numerical calculation of internally heated convection in an 8×1 box are shown in Fig. 5. Time is measured in units of d^2/κ and distance in terms of the depth d, where κ is the thermal diffusivity. The numerical method is described by Richter [18] and is used here for an internally heated, non-rotating, uniform viscosity, infinite Prandtl number fluid with boundary conditions:

$$T = 0, \psi \text{ and } \partial^2\psi/\partial z^2 = 0 \text{ on } z = 1 \text{ (top)} \quad (7)$$

$$\frac{\partial T}{\partial z} = 0, \psi \text{ and } \partial^2\psi/\partial z^2 = 0 \text{ on } z = 0 \text{ (bottom)} \quad (8)$$

$$\frac{\partial T}{\partial x} = 0, \psi \text{ and } \partial^2\psi/\partial x^2 = 0 \text{ on } x = 0, 8 \quad (9)$$

The Rayleigh number $Ra = g\alpha Hd^5/k\kappa\nu$ is the only parameter in the problem and the value used, 1.4×10^6 corresponds to upper mantle convection with an average heat flux out of the system of 5.85×10^{-2} W m^{-2} [14]. g is the acceleration of gravity, α is the coefficient of thermal expansion, H is the volumetric heating rate, d is the depth, k is the thermal conductivity, κ is the thermal diffusivity and ν is the viscosity.

Fig. 6 shows the dispersal with time of 399 particles originally uniformly distributed over a region one depth scale wide. The horizontal position of these particles as a function of time is shown in Fig. 7 and gives the impression of a diffusive process. The simplest parameterization of this process is obtained by assuming randomness for which [19]:

$$\sigma^2 = \kappa_e t \quad (10)$$

where σ is the second moment of the distribution about its mean position $\overline{X}$. Fig. 8 shows both $\overline{X}$ (in units of d) and σ^2 (in units of d^2) as a function of time (in units of d^2/κ). The effective diffusivity κ_e is estimated from the average slope of σ^2 vs. t giving:

$$\kappa_e \sim 30\kappa \quad (11)$$

which corresponds to a dimensional value $\kappa_e \sim 0.3$ cm^2/s (κ is typically estimated to be about 0.01 cm^2/s).

The effective diffusivity of many geophysical systems varies with scale and the value obtained depends on the separation of the particles used to determine it. In the atmosphere for example, particles a few meters apart might be seen to separate at rates giving an effective diffusivity of about 10^4 cm^2/s while those separated by several thousand kilometers would produce an estimate of the order of 10^{11} cm^2/s [20]. The relative motion of parsnip floating in the sea was found by Richardson and Stommel [21] to suggest a diffusivity that depends on their separation l as $l^{1.4}$. The earth's mantle is potentially as complicated as the ocean or atmosphere in so far as the dispersal of heterogeneities is concerned, but in what follows we parameterize the process in terms of a scale-independent effective diffusivity. We did test the effective diffusivity of the internally heated case using Richardson's [20] distance-neighbor method, and found no significant variation with scale. Apparently, the detachment of cold plumes from the upper boundary layer is sufficiently random to produce a reasonably uniform effective diffusivity, which could be used to describe the stirring of passive chemical species in the interior of a planetary body without plate tectonics.

However, our interest is really the earth and so the exercise that follows should be seen as the first of a hierarchy of models that may eventually contribute to a rational basis for discussing the evolution of chemical heterogeneities in the earth's mantle.

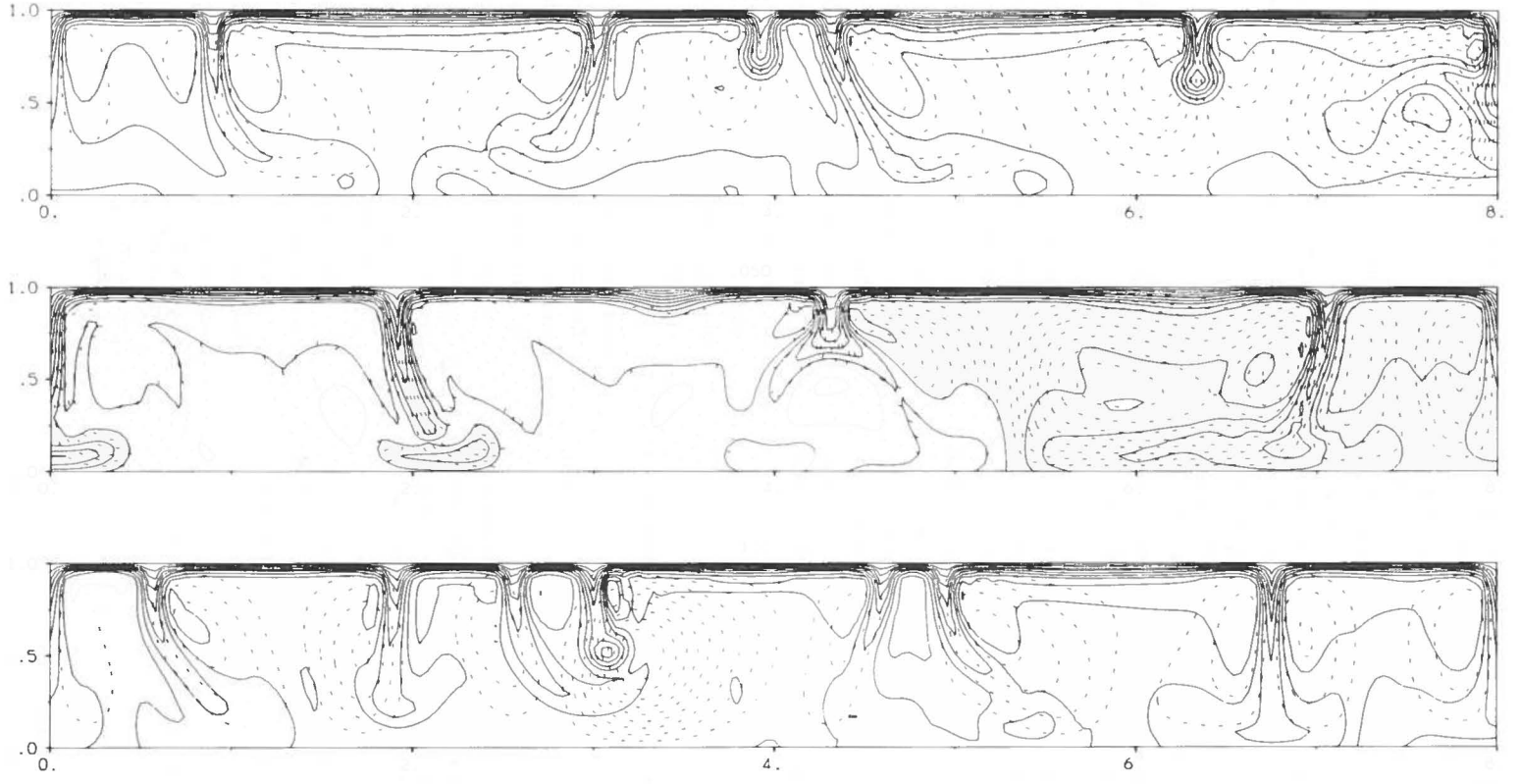

Fig. 5. Isotherms (solid lines) and the streamlines (dashed lines) at three different times (0, 0.05 and 0.1 in units $d^2\ \kappa$) in internally heated convection at $Ra\quad 1.4\times 10$.

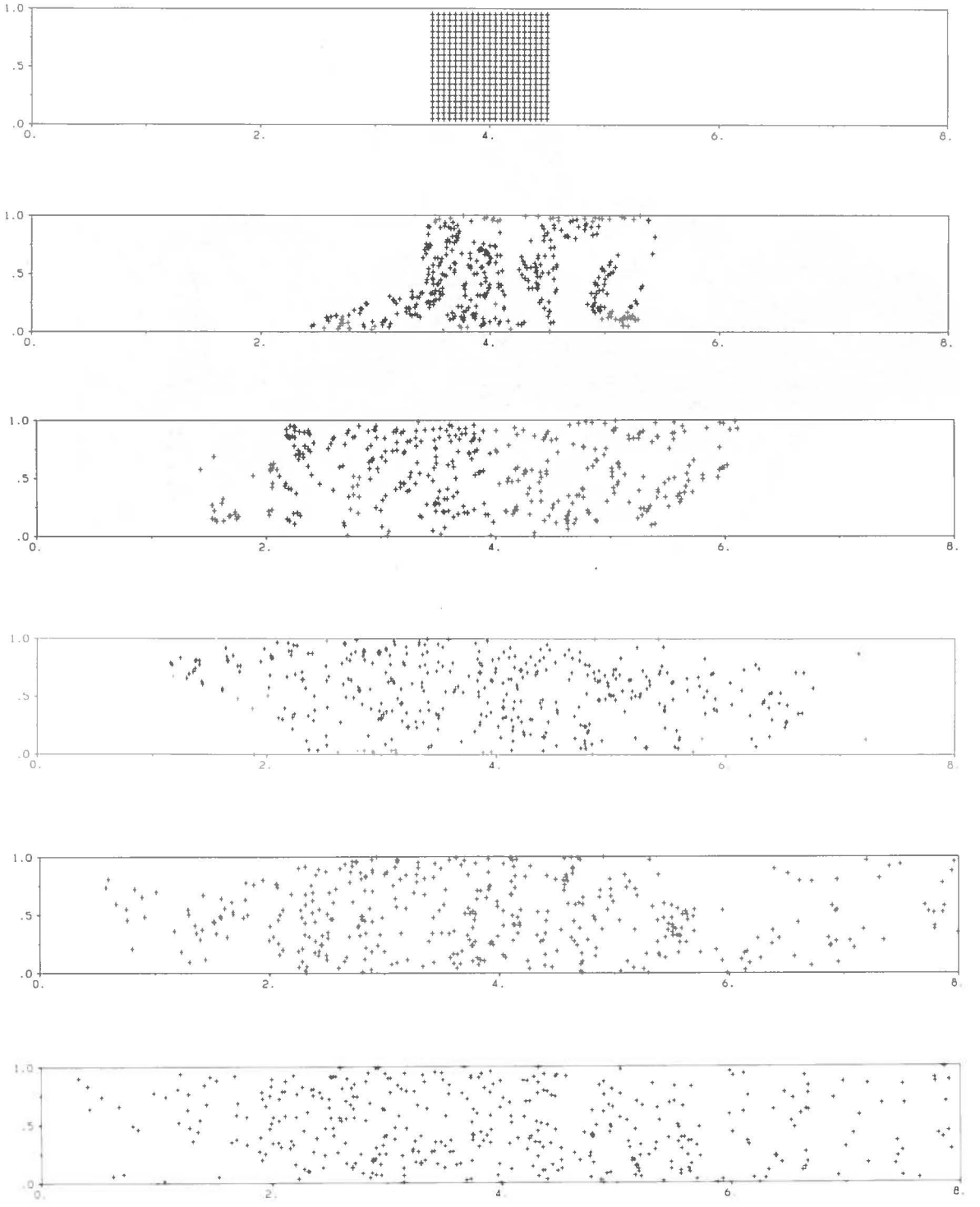

Fig. 6. Position of 399 particles advected by the flow shown in Fig. 5. From top to bottom times are from 0 to 0.1 in increments of 0.02 d^2/κ.

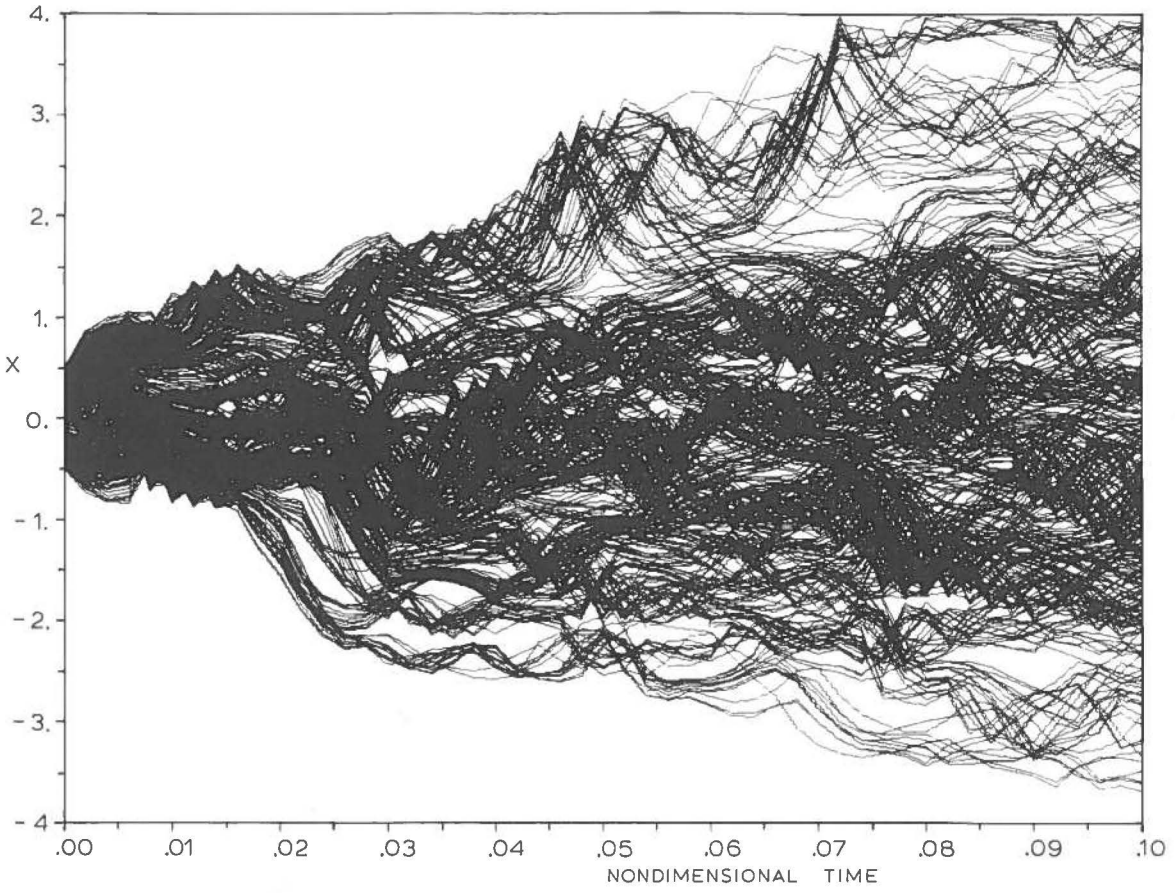

Fig. 7. The x position (in units of d) of the 399 particles as a function of time in units of d^2/κ.

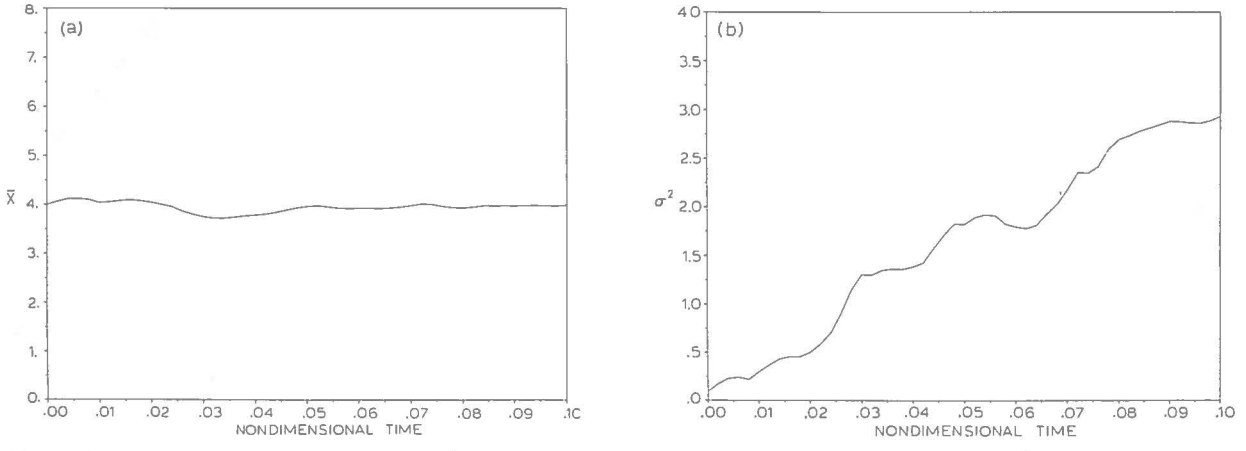

Fig. 8. First (a) and second (b) moment, $\bar{x}$ and σ^2, of the particle distribution as a function of time in units of d^2/κ. The average slope of the second moment gives the effective diffusivity in units of the thermal diffusivity.

5. Isotopic evolution in a convecting layer

The essentials of the model problem are as follows. An initially uniform reservoir (UR) suffers a single melting event at time t. The degree of melting, $F(x)$, varies spatially about a mean F_0, which was chosen such that in the absence of spatial variations it would produce good agreement with the average observed isotopic composition of MORB. $F(x)$ produces horizontal variations in each chemical specie but initially there is no variability in the isotopic ratios. However, since the parent to daughter ratios are not spatially uniform, variations in the isotopic ratios do develop with time. The magnitude of this variation as a function of time depends on the competing effect of production by decay opposed by the stirring effect of convection, which we parameterize as an eddy diffusivity.

This model problem, which is based on Jacobsen and Wasserburg's [5] model I, involves several levels of abstraction. To begin with the melting and removal of melt from the mantle is not meant to represent any particular real process and is used simply as a way of specifying elemental fluxes out of the mantle such that the residual mantle and continental crust have the desired concentrations and subsequent isotopic evolution. We are therefore using an effective degree of melting and effective partition coefficients that we hope embody the consequences but not the process of extracting the continental crust. This is taken a step further by assuming that the effective degree of melting is spatially variable, but in fact we could have just as well specified variations in the elemental concentrations directly. The use of a melting function is simply to produce variations for the different elements that are correlated in a way justified by the existing geochemical data. Finally we have assumed that the extraction of the continental crust occurs at a single time equal to the mean age of the continents even though a continuous evolution is much more realistic. The simpler single-stage model is sufficient for our present purpose, which is to illustrate some general effects of convectively stirring an isotopically evolving system.

UR has concentration C_{i0} (Table 1) of each specie and a corresponding number of atoms N_{i0} per unit volume. The subscript $i = \mathrm{s}$ represents a stable reference isotope, $i = \mathrm{r}$ represents a radioactive parent with decay constant λ, and $i = \mathrm{d}$ represents the daughter of r of the same element as s.

The evolution of UR is given by:

$$\left(\frac{N_{\mathrm{d}0}}{N_{\mathrm{s}0}}\right)_t = \left(\frac{N_{\mathrm{d}0}}{N_{\mathrm{s}0}}\right)_0 + \left(\frac{N_{\mathrm{r}0}}{N_{\mathrm{s}0}}\right)_0 (1 - \mathrm{e}^{-\lambda t}) \tag{12}$$

and:

$$\left(\frac{N_{\mathrm{r}0}}{N_{\mathrm{s}0}}\right)_t = \left(\frac{N_{\mathrm{r}0}}{N_{\mathrm{s}0}}\right)_0 \mathrm{e}^{-\lambda t} \tag{13}$$

where the assumed initial ratios for the Sm-Nd and Rb-Sr systems are given in Table 1.

At $t_0 = 2.75 \times 10^9$ years ($t_0 = 2.75 \times 10^9$ years and $F_0 = 1.78\%$ are based on Jacobsen and Wasserburg's [5] model I) UR is partially melted according to:

$$F(x) = F_0\left[1 + \frac{2\gamma}{\pi}\sum_{n=1}^{\infty}\frac{1}{(2n+1)}\sin\left\{\frac{(2n+1)\pi x}{L}\right\}\right] \tag{14}$$

This corresponds to a square wave with mean F_0, range γF_0 and wavelength $2L$. Fig. 9 shows the melting function for $\gamma = 0.5$, the value used below. Assuming equilibrium partial melting the concentrations in the residual mantle are:

$$C_i(x) = \frac{C_{i0} D_i}{F(x) + D_i\{1 - F(x)\}} \tag{15}$$

The values used for the partition coefficients D_i are given in Table 1. From (15) and knowing the isotopic composition of UR at t, the atomic concentration $N_i(x)$ can be found. Both $C_i(x)$ and $N_i(x)$ are square waves and we can write:

$$N_i(x, t_0) = \bar{N}_i - \frac{2\Delta N_i}{\pi}\sum_{n=0}^{\infty}\frac{1}{(2n+1)} \times \sin\left\{\frac{(2n+1)\pi x}{L}\right\} \tag{16}$$

where $\bar{N}_i$ and ΔN_i are the average and range of $N_i(x)$ which are given in Table 2 for the Sm-Nd and Rb-Sr systems.

The equations governing the evolution of $N_i(x, t)$ in a deforming system are:

$$\frac{\partial N_i}{\partial t} + \underset{\sim}{u} \cdot \nabla N_i = -\lambda_i N_{\mathrm{r}} \tag{17}$$

TABLE 1

Values used in calculations *

	C_{i0}	D_i	λ_i	$(N_{d0}/N_{s0})_0$	$(N_{r0}/N_{s0})_0$	$(N_{d0}/N_{s0})_{4.55}$	$(N_{r0}/N_{s0})_{4.55}$
Rb	0.645	0.0013					
^{87}Rb			0.0142				
Sr	22	0.043			0.0882		0.08268
^{86}Sr							
				0.698982		0.7045	
^{87}Sr							
Sm	0.41	0.065					
^{147}Sm			0.00654				
Nd	1.26	0.032			0.19945		0.1936
^{144}Nd							
				0.50599		0.511836	
^{143}Nd							

* λ is in aeons^{-1}. $(N_{d0}/N_{s0})_0$ and $(N_{r0}/N_{s0})_0$ are daughter to stable and radioactive parent to stable ratios 4.55×10^9 years ago ($t=0$). $(N_{d0}/N_{s0})_{4.55}$ and $(N_{r0}/N_{s0})_{4.55}$ are the corresponding present-day values. Values based on Jacobsen and Wasserburg [5].

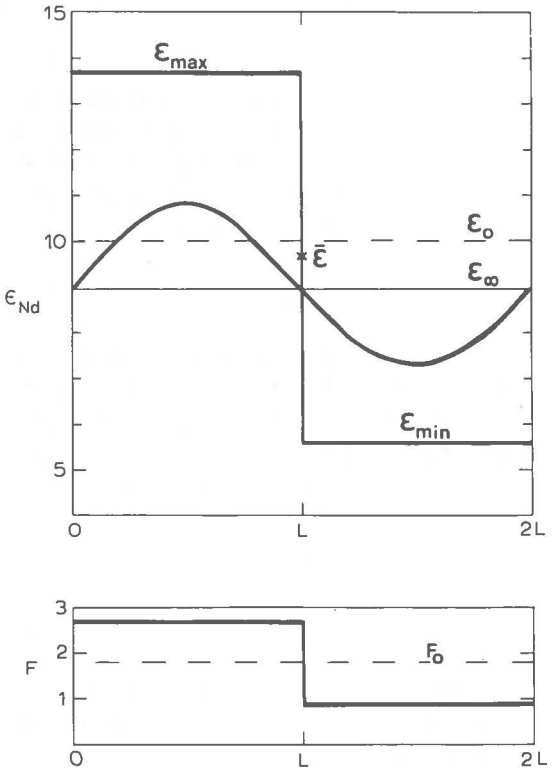

Fig. 9. The percent melt with mean F_0 and total range γF_0 is shown in the lower graph. The resulting ϵ_{Nd} values of the residual material 1.8×10^9 years after extraction of melt for different values of κ_e are shown in the upper panel. The square wave results when $\kappa_e=0$ and has an average ϵ value of $\bar{\epsilon}$. ϵ_∞ is the value for $\kappa_e=\infty$ representing complete mixing. The almost sinusoidal variation is for $\kappa_e=0.3$ cm^2/s and a length scale L of 4000 km. ϵ_0 is the value obtained if a uniform $F=F_0$ is used.

where:

$$\lambda_i=\begin{cases}1, i=\mathrm{r}\\ -1, i=\mathrm{d}\\ 0, i=\mathrm{s}\end{cases}$$

and u is the Eulerian velocity field. Based on the results of the previous section we replace the advection term by a diffusion term with diffusivity κ_e. Thus (17) becomes:

$$\frac{\partial N_i}{\partial t}=\kappa_e\frac{\partial^2 N_i}{\partial x^2}-\lambda_i N_r \tag{18}$$

subject to the initial conditions given by (16). Solutions are:

$$N_r(x,t)=\bar{N}_r e^{-\lambda\tau}-\frac{2\Delta N_r}{\pi}\sum_{n=0}^{\infty}\frac{1}{(2n+1)}\times\sin\left\{\frac{(2n+1)\pi x}{L}\right\}e^{-\phi_n\tau} \tag{19}$$

$$N_s(x,t)=\bar{N}_s-\frac{2\Delta N_s}{\pi}\sum_{n=0}^{\infty}\frac{1}{(2n+1)}\times\sin\left\{\frac{(2n+1)\pi x}{L}\right\}e^{-\phi_n\tau} \tag{20}$$

TABLE 2

Results of the calculations with $F_0 = 1.78\%$, $\gamma = 0.5$ *

	$N_{i\,\min}$	$N_{i\,\max}$	$\bar{N}_i$	ΔN_i	$f_{\min}$	$f_{\max}$	$\bar{f}$	f_0
^{87}Rb	0.005505	0.0151105	0.0103078	0.0096054	−0.926	−0.847	−0.880	−0.905
^{86}Sr	0.875753	1.165329	1.020541	0.289576	(−28.1)	(−25.7)	(−26.8)	(−27.5)
^{87}Sr	0.615096	0.818482	0.716789	0.203386				
^{147}Sm	0.217740	0.267165	0.242452	0.049425	0.306	0.125	0.200	0.225
^{144}Nd	0.851066	1.212118	1.031592	0.361052	(13.7)	(5.6)	(8.9)	(10.0)
^{143}Nd	0.433656	0.617628	0.525642	0.183972				

* The atomic abundances have been normalized such that N_i for ^{86}Sr and ^{144}Nd are one when $F(x) = F_0$. f is the enrichment factor for the minimum, maximum, and mean atomic concentrations. The value in parentheses is the corresponding present-day ϵ value.

$$N_d(x,t) = \bar{N}_d + \bar{N}_r(1 - e^{-\lambda\tau}) - \frac{2}{\pi}\{\Delta N_d + \Delta N_r(1 - e^{-\lambda\tau})\} \sum_{n=0}^{\infty} \frac{1}{(2n+1)} \times \sin\left\{\frac{(2n+1)\pi x}{L}\right\} e^{-\phi_n \tau} \quad (21)$$

where $\tau = t - t_0$ and $\phi_n = (2n+1)^2\pi^2\kappa_e/L^2$. The results are most usefully given in terms of ϵ units defined as:

$$\epsilon(x,t) = \left[\left\{\frac{N_d(x,t)}{N_s(x,t)}\right\} \Big/ \left\{\frac{N_{d0}(t)}{N_{s0}(t)}\right\} - 1\right] \times 10^4 \quad (22)$$

In evaluating expressions (19) to (21) for finite κ_e we will neglect all terms in the summation other than the first. This approximation is acceptably accurate when:

$$\tau > L^2 \times 10^{-18} (10^9 \text{ years/cm}^2) \quad (23)$$

Fig. 9 shows the results for present-day ϵ_{Nd} when L is 4000 km, t_0 is 2.75×10^9 years and κ_e is 0, ∞, or 0.3 cm^2/s. The dashed line marked ϵ_0 is the ϵ value for uniform partial melting given by model I of Jacobsen and Wasserburg [5]. The case $\kappa_e = 0$ involves no stirring by convection and results in a square wave with average $\bar{\epsilon}$ ($\neq \epsilon_0$). $\kappa_e = \infty$ is the limit of very efficient stirring for which all variations are suppressed (after 1.8×10^9 years) and produces a constant ϵ value ϵ_∞, which is significantly lower than ϵ_0. The results for ϵ_{Sr} are comparable but of much smaller amplitude. The various mean values of ϵ_{Nd} and ϵ_{Sr} are given in Table 2.

The difference between ϵ_∞ and ϵ_0 shows that a model with spatial variations and efficient stirring is not equivalent to a uniform model with the same average degree of melting. The exact meaning of the average observed ϵ value is seen to be somewhat complicated even in the present case when all the melt is extracted at a single time. Models in which the continental crust accumulates through time will be the subject of a separate paper.

The total range of ϵ values as a function of time for different choices of L is given in Figs. 10 and 11. A simple but accurate approximation for ϵ_∞ and $\Delta\epsilon$ is given by:

$$\epsilon_\infty = q\bar{f}(1 - e^{-\lambda\tau}) \quad (24)$$

and

$$\Delta\epsilon = \frac{4}{\pi} q\,\Delta f (1 - e^{-\lambda\tau}) e^{-\pi^2\kappa_e\tau/L^2} \quad (25)$$

where $\Delta\epsilon$ is the total variation of ϵ and:

$$q = 10^4 \left(\frac{N_{r0}}{N_{s0}}\right) \Big/ \left(\frac{N_{d0}}{N_{s0}}\right) \quad (26)$$

$$\bar{f} = \left(\frac{\bar{N}_r}{\bar{N}_s}\right) \Big/ \left(\frac{N_{r0}}{N_{s0}}\right) - 1 \quad (27)$$

$$\Delta f = f_{\max} - f_{\min} = \frac{2\gamma F_0(\delta_s - \delta_r)}{(F_0\delta_r + 1)^2 - (\gamma F_0 \delta_r)^2} \quad (28)$$

$$\delta_s = \frac{1 - D_s}{D_s}\,;\ \delta_r = \frac{1 - D_r}{D_r} \quad (29)$$

Equation (24) is commonly used [5] while (25) shows that $\Delta\epsilon$ is simply the total possible range of

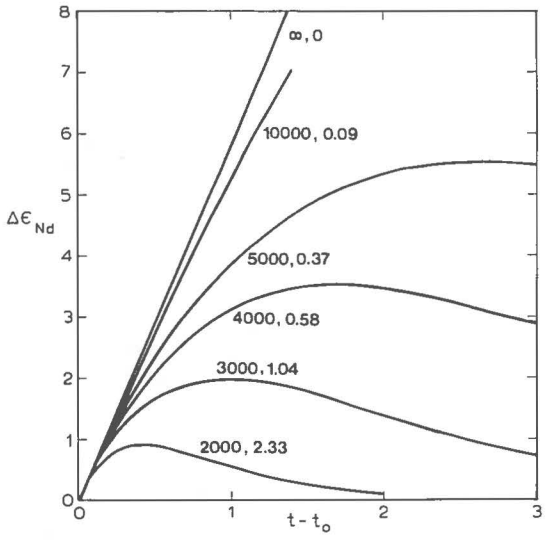

Fig. 10. The total variation ($\Delta\epsilon_{Nd}$) of ϵ_{Nd} as a function of time since melting (in 10^9 years) for different choices of length scale L and $\kappa_e = 0.3$ cm^2/s. The first value by each curve is L in kilometers. The second number is $\pi^2\kappa_e/L^2$, which is the real quantity controlling the evolution of $\Delta\epsilon_{Nd}$.

ϵ (from the difference between the maximum and minimum enrichment factors f_{max} and f_{min}) times an exponentially decaying term representing the effect of the effective diffusivity. The $4/\pi$ comes from the first term in the sine series of a square wave.

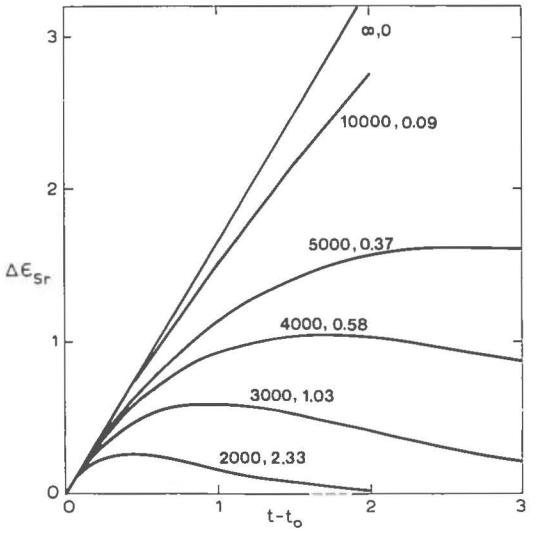

Fig. 11. Same as Fig. 10 but for Sr.

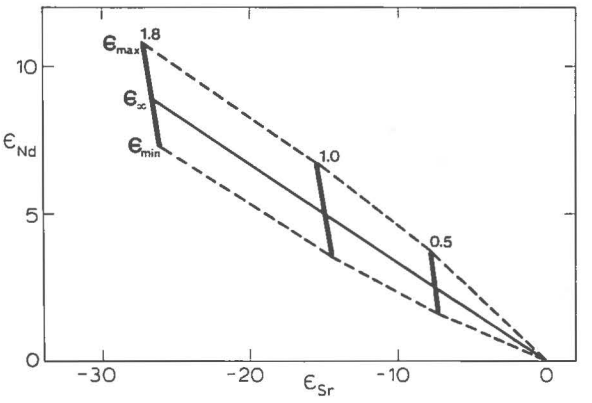

Fig. 12. ϵ_{Nd} vs. ϵ_{Sr} at different times in units of 10^9 years. The heavy almost vertical lines show the range of ϵ values at each time when $L = 4000$ km and κ_e is 0.3 cm^2/s. The straight line is the evolution curve for ϵ_∞ and the dashed curves give the envelope of the ϵ variations.

The results given in Figs. 10 and 11 are for the evolution of a periodic heterogeneity of wavelength $2L$ which should not be confused with the evolution of a localized heterogeneity. The localized case requires first decomposing the variations in the enrichment factor f into its Fourier components $\hat{f}(m)$, where m is the wavenumber. For each wavenumber there is then an equation like (25):

$$\hat{\epsilon}(m) = q\hat{f}(m)(1 - e^{-\lambda\tau})e^{-m^2\kappa_e\tau} \qquad (30)$$

where $\hat{\epsilon}(m)$ is the Fourier transform of the variations in ϵ at time τ. The effective diffusivity acts as a spectral attenuator damping only the large wavenumber (short wavelength) components of ϵ.

Fig. 12 gives the range of ϵ_{Nd} and ϵ_{Sr} at three different times, and also illustrates how ϵ_∞ will move along the correlation line (for appropriate values of the enrichment factors) but that the variations in ϵ are along trends different from the correlation line. This is due to the fact that equilibrium partial melting models with reasonable partition coefficients do not produce changes in ϵ (due to variations in F) that lie on the correlation line [7].

6. Summary and discussion

We began with examples of the stirring of a passive tracer by steady convection to illustrate the

need for time dependence if dispersal is to be over scales large compared to the individual cells. We chose as a reasonable model for the required time dependence the case of internally heated convection, which can be generalized to be representative of flows in which the position of the cells changes on a time scale comparable to the turnover time. Such a flow disperses an initially concentrated set of particles in a way that we characterized as diffusive and for Rayleigh number 10^6 we obtain a coefficient of effective diffusivity of 0.3 cm^2/s.

The use of a diffusivity, be it molecular or effective, implies a willingness to sacrifice a certain amount of detail for the sake of an economical description. There is always an implicit length scale below which the representation breaks down, and thus, its usefulness can only be judged in the context of a particular problem. In the case of isotopic variations in the mantle, the relevance of an effective diffusivity will depend on the initial conditions, the statistical properties of the convective flow and most importantly on the size of the region providing melt that eventually is erupted at the surface. The draining of melt from a volume of partially melted source is an averaging process that will result in lavas whose isotopic composition reflects the properties of the entire source volume, a volume that may be sufficiently large to justify the diffusive representation. The numerical experiment using internally heated convection suggests that the system will appear diffusive after 2×10^9 years if the volume sampled has dimensions of about one tenth the layer depth. If sampled on a smaller scale, the full range of isotopic compositions could still be observed since convection redistributes but does not erase the variations. Ultimately, the question of whether the evolution of chemical heterogeneities in the mantle can be sensibly discussed in terms of an effective diffusivity will only be determined from the isotopic data itself once a sufficiently large number of samples have been analysed. For the moment, one can say that the diffusive representation is more likely to be useful if the relevant convective flow is restricted to the upper mantle where the sampling volume will have to be of the order of 50–100 km in typical dimensions and for mid-ocean ridge data where the zone drained of partial melt could easily be of sufficiently large size.

We used an effective diffusivity to represent the dispersal of chemical heterogeneities caused by the extraction of the "continental crust" from a primitive uniform "mantle". The model is a variation on Jacobsen and Wasserburg's model I, the main difference being that the degree of melting is now spatially variable (around a mean value that alone would produce the results of model I). The averaged ϵ values measured in such a system depend not only on the average degree of melting but also on the variation in partial melt and thoroughness of convective stirring, and are always different than the result of model I. This is due to the non-linear dependence of the residual concentration on the degree of melting and the fact that if there is no mixing the averaged ϵ value is a simple average while after mixing the system has a uniform ϵ value that is a concentration weighted average. In general, models assuming a uniform degree of melting are not applicable to a situation with variable melting and subsequent homogenization by convection.

The evolution of variations $\Delta\epsilon$ around the mean ϵ_∞ depends on the range of enrichment factors, which provide an upper bound for $\Delta\epsilon$, and an exponential decay ($e^{-\pi^2\kappa_e\tau/L^2}$), which determines what fraction of the bound is achieved. The dependence of this decay on the characteristic length scale associated with the initial heterogeneity is possibly the most serious limiting factor in answering the question of whether variations associated with continental extraction should still be seen in present data. On the other hand, such a decay suggests that the spatial spectrum of $\Delta\epsilon$, which becomes increasingly biased towards long wavelengths, might provide a test of the concept of an effective diffusivity when applied to the mantle.

Acknowledgments

We thank Dan McKenzie and Peter Rhines for comments, often blunt, on various topics covered in this paper. We also would like to thank Barry Lesht for providing us with a copy of the Richardson and Stommel paper. F.M.R. thanks the Royal Society for a Guest Research Fellowship allowing

him to visit Cambridge University where this work was finished. His research is also supported by the National Science Foundation grant NSF-EAR 79-26482. S.F.D. was supported at the Jet Propulsion Laboratory, California Institute of Technology, by a grant from the Geodynamics Program office of NASA under contract NAS7-100. The numerical calculations were done at the National Center for Atmospheric Research, which is supported by N.S.F. Grant EAR 79-26482.

References

1 D.J. DePaolo and G.J. Wasserburg, Nd isotopic variations and petrogenetic models, Geophys. Res. Lett., 3 (1976) 249.
2 D.J. DePaolo and G.J. Wasserburg, Inferences about magma sources and mantle structure from variations in $^{143}Nd/^{146}Nd$, Geophys. Res. Lett. 3 (1976) 743.
3 P. Richard, N. Shimizu and C.J. Allègre, $^{143}Nd/^{146}Nd$, a natural tracer: an application to oceanic basalts, Earth Planet. Sci. Lett. 31 (1976) 269.
4 R.K. O'Nions, P.J. Hamilton and N.M. Evenson, Variations in $^{143}Nd/^{144}Nd$ and $^{87}Sr/^{86}Sr$ ratios in oceanic basalts. Earth Planet. Sci. Lett. 34 (1977) 13.
5 S.B. Jacobsen and G.J. Wasserburg, The mean age of mantle and crustal reservoirs, J. Geophys. Res. 84 (1979) 7411.
6 D.J. DePaolo, Nd isotopic studies: some new perspectives on earth structure and evolution. EOS, Trans. Am. Geophys. Union 62 (1981) 137.
7 D.J. DePaolo, Implications of correlated Nd and Sr isotopic variations for the chemical evolution of the crust and mantle, Earth Planet. Sci. Lett. 43 (1979) 201.
8 C.J. Allègre, D. Ben Othman, M. Polvé and P. Richard, The Nd-Sr isotopic correlation in mantle materials and geodynamic consequences, Phys. Earth Planet. Inter. 19 (1979) 293.
9 F.M. Richter and N.M. Ribe, On the importance of advection in determining the local isotopic composition of the mantle, Earth Planet. Sci. Lett. 43 (1979) 212.
10 F.M. Richter, Convection and the large scale circulation of the mantle, J. Geophys. Res. 78 (1973) 8735.
11 F.M. Richter and B. Parsons, On the interaction of two scales of convection in the mantle, J. Geophys. Res. 80 (1975) 2529.
12 D.P. McKenzie, Finite deformation during fluid flow, Geophys. J.R. Astron. Soc., 58 (1979) 689.
13 R.J. O'Connell and B. Hager, Differentiation in a convecting mantle, EOS, Trans. Am. Geophys. Union 60 (1979) 935.
14 D.P. McKenzie, J.M. Roberts and N.O. Weiss, Convection in the earth's mantle: towards a numerical simulation, J. Fluid Mech. 62 (1974) 465.
15 S.F. Daly, Convection with decaying heat sources: constant viscosity, Geophys. J.R. Astron. Soc., 62 (1980) 519.
16 R.K. O'Nions, N.M. Evensen, P.J. Hamilton and S.R. Carter, Melting of the mantle past and present: isotope and trace element evidence, Philos. Trans. R. Soc. London, 258 (1978) 547.
17 F.M. Richter and D.P. McKenzie, On some consequences and possible causes of layered mantle convection. J. Geophys. Res., 86 (1981) 6133.
18 F.M. Richter, Dynamical models for sea floor spreading, Rev. Geophys. Space Phys. 11 (1973) 223.
19 A. Einstein, Über die von der molekularkinetischen Theorie der warmen geforderten Bewegung von in ruhenden Flüssigkeiten suspendierten Teilchen, Ann. Phys. 17 (1905) 549.
20 L.F. Richardson, Atmospheric diffusion shown on a distance-neighbour graph, Proc. R. Soc. London, 110 (1926) 709.
21 L.F. Richardson and H. Stommel, Note on eddy diffusion in the sea, J. Meteorol. 5 (1948) 238.
22 D.J. DePaolo and G.J. Wasserburg, Petrogenetic mixing models and Nd-Sr isotopic patterns, Geochim. Cosmochim. Acta, 43 (1979) 615.